Наносистеми, наноматеріали, нанотехнології
Nanosistemi, Nanomateriali, Nanotehnologii
2025, т. 23, № 3, сс. 677–718
https://doi.org/10.15407/nnn.23.03.0677

PACS numbers: 61.05.cp, 68.55.J-, 73.61.Le, 78.30.Hv, 78.55.Hx, 78.67.Bf, 81.07.Bc

A Review on Synthesis and Characterization of Some Copper-Oxide Properties and Potential Application

Kenza Almi, Maria Nor Elyakin Boumezrag, and Said Lakel

Laboratory of Metallic and Semiconducting Materials,
University of Biskra,
07000 Biskra, Algeria

This review focuses on the synthesis and characterization of *p*-type metal-oxide (*p*-type CuO) semiconductor thin films used for chemical-sensing applications. *p*-Type CuO thin film exhibit several advantages over *n*-type metal-oxide, including a higher catalytic effect, low humidity dependence, and improved recovery speed. However, the sensing performance of CuO thin film is strongly related to the intrinsic physicochemical properties of the material and their thickness. The latter is heavily dependent on synthesis techniques. Many techniques used for growing *p*-type CuO thin film are reviewed herein. Copper oxide is called a multifunctional material by dint of possessing a broad range of the chemical and physical properties, which are often highly sensitive to changes in processing parameters, although, extensive research and development, the optimization of the processing parameters are still in full development until today, where the overall research found that the different properties of copper oxide are based on the experimental conditions. In this extensive review, we focus more on discussing the effect of major synthesis processing parameters such as precursor solution, annealing temperature, and thickness of the nanomaterial, which various researchers have obtained. These factors are critical overviewed, evaluated, and compared.

Цей огляд зосереджений на синтезі та характеризації тонких напівпровідникових плівок на основі металооксиду *p*-типу (CuO *p*-типу), що використовуються для хемічної сенсибілізації. Тонкі плівки CuO *p*-типу мають ряд переваг над металооксидом *n*-типу, включаючи вищий каталітичний ефект, низьку залежність від вологости та поліпшену швидкість відновлення. Однак сенсорна продуктивність тонкої плівки CuO тісно пов'язана з власними фізико-хемічними властивостями матеріялу та його товщиною. Остання сильно залежить від методів синтези. Тут розглянуто багато методів, що використовуються для вирощування тонкої плівки CuO *p*-типу. Оксид Купруму називають багатофункціональним матеріялом завдяки широкому спектру хемічних і фізичних

властивостей, які часто дуже чутливі до змін параметрів оброблення, хоча завдяки широким дослідженням і розробкам оптимізація параметрів оброблення все ще перебуває в повному розвитку дотепер. Загальні дослідження показали, що різні властивості оксиду Купруму залежать від експериментальних умов. У цьому розширеному огляді ми більше зосереджуємося на обговоренні впливу основних параметрів синтези, таких як розчин-провісник, температура відпалу та товщина наноматеріялу, які вже одержали різні дослідники. Ці чинники критично розглянуто, оцінено та порівняно.

Key words: semiconductor copper oxide, synthesis methods, *p*-CuO thin films, precursor solution, annealing temperature.

Ключові слова: напівпровідниковий оксид Купруму, методи синтези, тонкі плівки *p*-CuO, розчин-провісник, температура відпалу.

(Received 24 December, 2023; in revised form, 27 December, 2023)

1. INTRODUCTION

In the technology industry, semiconductors are critical tools for nanoscale electrical transportation due to their physical and chemical properties. It is seen as a promising material due to its appropriate band gap and high absorption coefficient in the visible light region. Apart from good optical and electrical properties, the material has many advantages such as the availability and abundance of raw materials, the non-toxic nature and the low cost of production [1].

Among these materials copper oxide, which is a compound with the binary copper–oxygen system, contains two stable phases: Cu_2O (cuprite) and CuO (tenorite). In addition to these stable phases, a metastable one is also reported: Cu_4O_3 (paramelaconite) [2].

Different processes can be used to deposit copper oxide in thin films. One can note the chemical processes consist in elaborating the material by chemical reaction or molecule decomposition such as electrodeposition [3], chemical vapour deposition [4], SILAR [5], sol–gel [6]. Instead, the physical processes consist in developing the film by extracting the material from a target, for instance, sputtering [7], thermal oxidation [8], and plasma evaporation [9].

Cupric oxide (CuO) has attracted a lot of interest due to its fundamental and technological potential, especially, in several industries [10], where it has been employed as a basic material in photocatalytic reactions [11, 12], inertness sensors [13], nonenzymatic glucose sensors [14], ammonia sensing [15], antibacterial activity [16], oxide architectural pores [17], polymer solar cells [18], antifungal agents [19]; and CuO nanoparticles are also used in dry cell batteries as lithium-ion batteries [20, 21].

Developing a good quality material and mastering its structural, optical, and electrical properties are a major challenge. In this respect, the quest for the most efficient synthesis process, which yields not only large quantities but also high-quality and advanced material properties, continue.

The aim of this review devoted mainly to the properties of CuO thin films is to explain experimental-factors' consideration required during sample handling, and preparation according to the need imposed by the type of application; its beginning with the influences of preparation materials, until finished, form-ready samples, future research directions are also discussed.

2. INFLUENCE OF DEPOSITION PARAMETERS ON THIN FILM PROPERTIES

It will be illustrated the fundamentals of the synthesis of copper oxide with a particular focus on its influencing factors. Physical properties will be described depending on the method adopted in the preparation, and will be discussed stressing the consideration of the factors required during sample handling, preparation, and analysis.

2.1. Influence of Precursor Solution

The precursor solution is the first important process variable. Solvent, type of salt, concentration of salt, and additives influencing the physical and chemical properties of deposited film can be tailored by changing the composition of the precursor solution.

Figure 1 shows schematic diagram of the synthesis of CuO nanostructures.

2.1.1. Salt and Alkali-Metal Solution

In principle, any kind of soluble copper salt could be used as a precursor to prepare CuO nanostructures without much difference, or, at least, there seems to be less report on the effect of copper-salt precursor. Different copper salts such as chloride, nitrate, sulphate, and acetate were used to prepare CuO nanomaterials [22]. However, the influence of different copper salts was not discussed in detail. However, inorganic salts such as nitrates are often used, as precursors for sol–gel CuO-based materials, even though their main drawback is related to the inclusion or difficult removal of anionic species in the final product. Using copper acetate as a precursor, the acetate groups, as contaminants of the gel, decompose under annealing producing combustion volatile by-products [23]. Authors mentioned that the use of cop-

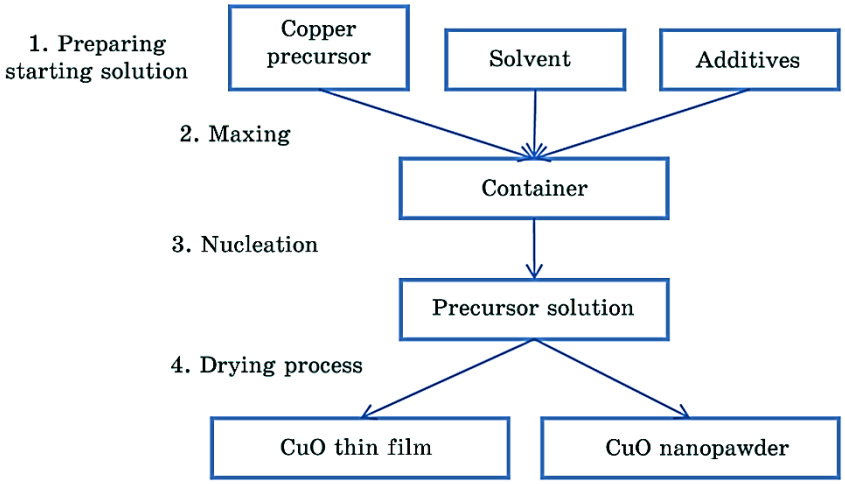

Fig. 1. Schematic diagram of the synthesis of CuO nanostructures.

per perchlorate instead of copper acetate yields a turbid suspension, *i.e.*, coagulation of the particles takes place [24]. This is also obtained, when using copper sulphate as a precursor [25]. The equations of the chemical paths of CuO deposition based on the various precursors in distilled water are as follow:

$$Cu(NO_3)_2 + H_2O \rightarrow CuO + 2HNO_3, \quad (1)$$

$$CuCl_2 + H_2O \rightarrow CuO + 2HCl, \quad (2)$$

$$(CH_3COO)_2 + H_2O \rightarrow CuO + 2CH_3COO. \quad (3)$$

In order to that, particle size and uniformity of copper nanoparticles prepared from copper acetate seem better than those from inorganic copper salt do. A reasonable explanation is that carboxylate groups are still adsorbed on the surface of the copper-oxide nanoparticles and play the role of a surfactant and suppress nanoparticles from growth and aggregating process [26].

2.1.2. Solvent

The term 'solvent' refers to a class of liquid organic chemicals of variable lipophilicity and volatility, small molecular size, and lack of charge, accordingly, which are frequently used to dissolve, dilute, or disperse materials, which are insoluble in water. Solvents are classified largely according to molecular structure or functional group. Classes of solvents include aliphatic hydrocarbons, many of which are chlorinated (*i.e.*, halocarbons), aromatic hydrocarbons, alcohols,

ethers, esters/acetates, amides/amines, aldehydes, ketones, complex mixtures that defy classification [27].

Indeed, one of the most crucial elements of wet chemical techniques is the solvent, where it has a noteworthy influence on the performance of the reaction and allows thermodynamic and kinetic control over a chemical reaction. It also greatly influences the stability and morphology of the synthesized particles; little consideration has been given to how the solvent affects alkoxides gels. This part of the review of published works on alkoxide sol–gel processing is pertaining to the role of the solvent. It is necessary to use a common solvent to being them into the solution [28].

Two primary criteria for the solvents used to synthesize CuO nanostructures are as follow:

(i) they dissolve copper and alkali hydroxide compounds;

(ii) they can be washed away easily or decomposed during the washing and drying process without leaving any detrimental impurities or residues in the final nanoproducts.

As seen in the following equation, copper-oxide nanoproducts are, as observed in the following Eq. (4), generated [29]:

$$\text{copper salt} + \text{alkaline hydroxide} \rightarrow \text{salt of alkaline metal} + Cu(OH)_2. \quad (4)$$

Alcohols are the most commonly used solvents. However, any family of organic liquids capable of hydrogen bonding with water can be employed, such as amines, amides, or ketones. Water was also used less in some reports, but without additives, which lower the surface tension and, thus, the appearance of defects. Researchers tend to use organic solvents. The majority of research on sol–gel processing has used methanol or ethanol as the solvent [30].

The synthesis process should pay close attention to a number of secondary parameters, including viscosity, surface tension, volatility, reactivity, toxicity, and cost.

Firstly, the use of these solvents imposes compliance with safety standards regarding their toxicity. The main determinants of a solvents' inherent toxicity are as follow:

(i) dimensional morphology: courser nanoparticles were lesser hazardous to finer ones;

(ii) facet charge: nanoparticles' toxicity is amplified by positive charge; this affirmative load uplifts the reactions amidst nanoparticles and cells;

(iii) dissolution: the CuO-nanoparticles' shattering is dependent on pH and temperature of the mixture and that influences their toxicity [31]; subtle differences in chemical structure can translate into dramatic differences in solvent toxicity [32] (*i.e.*, methanol, ethylene glycol, and isopropyl alcohol are referred that 'toxic alcohols') [33]; in fact, in

most of the reports, CuO nanoparticles were prepared by utilizing water as certainly the cheapest safest and most environmentally friendly solvent.

On the other hand, the hydrolysis and polymerization kinetics are impacted by the viscosity of the solvent, which alters the solution. A high viscosity will impede the reaction and lengthen the gelation period by reducing the mobility of the catalyst and reactants through the solution.

Increasing the viscosity ratio causes the particles to agglomerate. In the case of a highly viscous solvent, the viscosity resists particle movement. As a result, the particles keep their initial distribution [28, 34].

In another part, in the case of a solvent with a low viscosity, the solvent easily moves between the particles, and the surface tension then causes the particles to agglomerate. In the midst of the agglomerated particles, the solvent is prevented from evaporating consequently; the amount of available gel depends on the extent of the agglomeration.

Moreover, the surface tension σ of the used solution controls the droplet shape impact. Both solution surface tension and dissociation enthalpy alter the microstructure of the formed film as the surface tension σ increases, the connectivity of the pores decreases, and the structure increases. In the case of large surface tension, the surface tension overcomes the viscosity resistance and causes the particles to agglomerate. In the midst of agglomerated particles, evaporation stops, and, consequently, the remaining amount of gel increases.

As mentioned earlier, pure CuO films studied using different solvents affect the morphological properties [35, 36]. The using water as solvent larger particles of irregular shape and intricate structures as 3-dimensional structures were obtained [37–40]. Figure 2 shows the morphologies of copper oxides having different morphologies: (*a*) nanostructures, (*b*) nanowires, (*c*) nanostructures, (*d*) nanobelts, (*e*) nanostructures, (*f*) hollow spheres.

Noteworthy, they headed to use the organic solvent as a substitute. Among these solvents were the alcohols-synthesized CuO nanoparticles. Using a varied alcohol such as methanol, ethanol, and propanol exhibits more homogeneous surface, and decreasing in the grain size by using modified solvent was found to be comparable with a previous study [42].

In the same context, some research attributed the increase in the grain size in the films' synthesis by the alcohols' solvent to the increase of hydroxyl groups [43, 44].

Within this framework, the optical and electrical properties are also studied, but to lesser extent, most researches linked these changes to the type of solvent used. As reported by P. Mallick, the absorbance of CuO sample synthesized with propanol solvent shows faster exponential decrease indicating more strain generation in this case [45]. The behav-

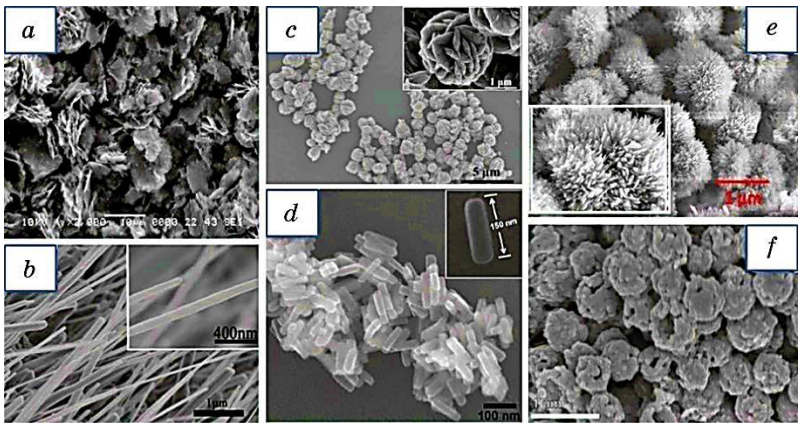

Fig. 2. Shows the morphologies of copper oxides having different morphologies: (*a*) nanostructures; (*b*) nanowires; (*c*) nanostructures; (*d*) nanobelts; (*e*) nanostructures; (*f*) hollow spheres.

iour of absorbance is typical for many semiconductors and can occur for a variety of reasons such as internal electric fields within the crystal, deformation of lattice due to strain caused by imperfection, and inelastic scattering of charge carriers by phonons [46]. Other study by N. Zayyoun focuses on the solvent effects using water, ethanol and propanol. They found that direct gap energy values were increased with decreasing particles' diameter of this solvents, accordingly [47]. There has been on other work in this filed by A. Y. Fasasi; using distilled water and ethanol, he have found that films produced using alcohol have more disordered states, and this manifest itself in the reduced band gap compared with that of aqueous samples; the values obtained are of 920 and 640 meV for CuO films from alcohol and distilled water-based precursors, respectively. The least attention was paid to the electrical properties as reported by A. Y. Fassasi; he has been observed that the values of resistivity recorded using ethanol as a solvent 21% are greater than the values obtained for the aqueous samples [48].

2.1.3. Additives

The formation of a stable sol is employed to simplify the complete dissolution of the precursor-alcoholic medium [51]. They act as base or acid and/or chelating agent. Alkali metal hydroxides, alkanolamines, alkylamines, carboxylic acids, acetylacetone and polyalcohols are used for this purpose [52].

The authors reported that the deposition efficiency and crystallinity of the films deposited by adding additives, which act as stabilizers or catalyst during the reaction, was improved.

TABLE 1. Summary on the effect of solvent on the properties of copper oxide.

Method	Precursors and synthesis conditions	Solvent	Morphology	Structure	Crystallite size [nm]	Band gap, eV
Sol–gel [45]	precursor: $Cu(NO_3)$, $2H_2O$ stirred: 1 h dried at 200°C calcined 300°C for 1 h, pellets were annealed at 500°C for 1 h	Ethanol propanol	nanoparticles	CuO monoclinic	28.57 nm 36.76 nm	direct band gap 1.18 eV 1.21 eV indirect gap ethanol and propanol 3.57 eV
Sol–gel [47]	(Cu $(CH_3COO)_2$, H_2O and NaOH stirring 2 h dried at 50°C	Propanol water ethanol	— needle-shaped and small spherical particles; — spherical and aligned along the c-axis; — spherical nanoparticles	CuO monoclinic crystal phase	9.5 nm 7 nm (about 4 nm)	direct band gap 4.2 eV 4.3 eV 4.9 eV
Sol–gel [49]	($Cu(NO_3)$, $3H_2O$) concentration of 0.1 M temperature up to 480°C	Methanol distilled water	methanol: interconnected structure with no distinguished grain boundaries and with separated pores over the whole surface; water: homogeneous surface of a dense structure.	CuO monoclinic crystal phase	by SEM grain size ranging from 40 to 160 nm from the water	2.13 eV for water, 2.18 for methanol

Continuation **TABLE 1.**

Method	Precursors and synthesis conditions	Solvent	Morphology	Structure	Crystallite size [nm]	Band gap, eV
Spray pyrolysis [48]	$CuCl_2$ concentration 0.1 M substrate, $T = 320$°C distance 23 cm annealing, $T = 500$°C	ethanol distilled water	No	CuO phase $Cu_{1.008}O_{0.992}$ $Cu_{0.956}O_{1.044}$, respectively	No	ethanol: 1.58 eV water: 1.79 eV
Photolysis [50]	potassium oxalate, copper sulphate stirring and heated at 60°C for 30 min cooled in ice water bath	water methanol ethanol	nanoparticles	CuO monoclinic	11.4 nm 10.8 nm 8.4 nm	4.21 4.47 4.58

D. S. C. Halin *et al.* have shown the addition of polyethylene glycol will increase the viscosity of solution due to chain length effects. Since the polyethylene glycol additive can avoid the particle aggregation occurring in the sol–gel solution, the grain size was reducing from 104 nm to 83 nm. Also, the addition of polyethylene glycol will produce crack free films with high optical absorbance [53], whereas, P. Samarasekara *et al.* demonstrated that ethylene glycol is a better additive compared with the polyethylene glycol [54].

Instead, hydroxide and potassium hydroxide are base agent which provides hydroxyl ion, which is strongly associated with reactions that form nanocrystals [55]. This explained by the increase in OH-ions with the pH, accelerating the process of CuOH formation Eq. (5) provoking a faster crystallization of Cu_2O Eq. (6) [56]:

$$Cu^+ + OH^- \rightarrow CuOH, \tag{5}$$

$$2CuOH \rightarrow Cu_2O + H_2O. \tag{6}$$

This fast crystallization reduces interstitial defects, allowing to the interstitial atoms move to the boundaries, relaxing the crystal and consequently reducing its size [57, 58].

Within the search of the authors, at bath pH ≅ 9.0, the (100) plane are produced and, in higher bath pH ≅ 11.0, the (111) are produced [59–61].

Other common additives are the alkanolamines, *i.e.*, monoethanolamine [MEA; $(HOCH_2CH_2)\ NH_2$] [62], diethanolamine [DEA; $(HOCH_2CH_2)_2NH$] [54], triethanolamine [TEA; $(HOCH_2CH_2)_3\ N$] [63] are the most widely used in the CuO thin film fabrication. Likewise, acetic acid (Ac. Ac.; CH_3COOH) [64] and lactic acid (Lactic Ac.; $CH_3CHOHCOOH$) [65] tartaric acid [66], oxalic acid [66], malic acid [66, 67] also added as complexing agent. Sometimes, it is preferable to use only a single additive in certain circumstance for better dissolution of the mixture.

As main results, used alcohols as a solvent implying produce an excellent characteristic and of nanostructure materials specially, when they are used with organic precursor, in addition if they are added to the additives they result from it more homogeneous layers, the alkanolamines are among the additives most compatibility with the result which mentioned earlier.

2.1.4. Molarity

Thin films and their properties are related to those of the initial solution [68, 69]. The used solution controls the crystallinity, film microstructure and optical properties.

Many studies investigated what effects molarity had on the structure, electrical and optical properties and surface morphology of the thin films. They concluded that, with the change in molar concentration the properties including density, porosity and gelation time are all significantly impacted consequently, the crystallite size varies, structural parameters change systematically, the shape of crystallites changes, the transmittance decreases [70, 71].

2.1.4.1. Structural Properties

Whatever, the precursor nature or the elaboration method, CuO thin films are generally polycrystalline in nature with monoclinic structure and XRD peaks corresponding to the (111), (002) this two main peaks at the angles $\cong 35.5°$ and $\cong 38.7°$ [74] and in some case, a small peak (110), $(\bar{2}00)$, (202), $(\bar{1}13)$, $(\bar{3}11)$, (220) with $2\theta = 32.52$, 48.74, 58.30, 61.56, 66.25, 68.13, respectively [72]. Most studies conducted on the impact of focus on synthesis have found that there is a relationship between the vary concentrations and structural parameters. There are observed an increase in peak intensity and a narrowing in width with increasing molarity of precursor solution. Furthermore, the strain decreased with the increase of molarity, reflecting the decrease of cohesive force in the film–glass interface. Specifically, low concentration results in no supersaturation, whereas high concentration results in higher supersaturation and aggregation of small size nuclei to form large particles and favours the nucleation under heterogeneous system [73].

2.1.4.2. Optical and Electrical Properties

Indeed, a maximum transparency in the visible region was showed for the lower concentration values, while it is increasing with this last.

The absorption edge in the transmittance spectra of the thin films shifts towards higher wavelength region by the increasing of molarity.

Photoluminescence (PL) spectra are required to investigate the levels and amounts of defects in CuO thin films.

In one case, they found the spectrum is composed mainly of a small and sharp peak located at 668 nm (1.86 eV) and a red broad one located at the 723 nm. The former peak is associated to the band-to-band transition since its energy is close to the value of the CuO bandgap. However, the red peak originates from the defects localized in the forbidden band of CuO material such as single ionized oxygen vacancy, the red peak intensity was enhanced with increasing the salt concentration suggesting that increasing the salt molarity leads to the formation of larger concentration of electronic point defects in CuO thin films [73].

TABLE 2. Summary on the effect of molarity on the properties of copper oxide.

Method	Precursors and synthesis conditions	Molarity, M	Structure	Crystallite size [nm]	Band gap, eV	Other parameters
Spray pyrolysis [72]	$Cu(NO_3)_2.3H_2O$ distilled water substrate temperature: 350°C the flux was maintained at 2 ml·min^{-1} the distance between the nozzle and the substrates was fixed at 20 cm	0.05 0.1 0.2 0.3	CuO phase CuO phase with Cu_2O phase	19 20 28 16	No	the contact angle measurement revealed that all the deposited films are hydrophobic, with contact angles 103.4°, 108.9°, 114° and 121° respectively with increasing of molarity; the thickness increases from 20 to 110 nm as the precursor concentration increases from 0.05 to 0.2 M, a decrease in film thickness for 0.3 M to around 75 nm; the electrical resistances 109, 54, 57 and 20 kΩ, respectively; gas sensing measurements confirm that 0.05 M sample is sensitive to different CO_2 concentrations; the gradual disappearance of porosity makes 0.2 M and 0.3 M films less sensitive; the porous structure disappears for 0.1, 0.2 and 0.3 M; the surface of the film shows regular distribution of tubular like shape pores for 0.05 M

Continuation **TABLE 2.**

Method	Precursors and synthesis conditions	Molarity, M	Structure	Crystallite size, [nm]	Band gap, eV	Other parameters
Sol–gel spin-coating method [73]	$[(CH_3COO)_2{\cdot}Cu/H_2O]$ 2-methoxyethanol $[C_3H_8O_2]$ diethanolamine $[NH(CH_2CH_2OH)_2]$ a speed of 4000 rpm for 30 s annealed at temperature 550°C for 1 h	0.1 0.3 0.5	polycrystalline nature with monoclinic structure of CuO	crystallites size increase with increasing the molar concentration	3.68 eV 2.56 eV 2.44 eV	thickness 132, 175 and 252nm respectively; the resistivity value increases slightly from 84 Ω cm to 124 Ω cm with the molar concentration
Spray pyrolysis [77]	$(CuCl_2, 2H_2O)$, double distilled water; substrate temperature: 400°C, carrier gas: compressed air rate of spray: 4ml/m; angular distance: 25cm	0.05 0.1 0.15	CuO thin films are polycrystalline in nature	13 17 23	1.76 1.50 1.45	

Continuation **TABLE 2.**

Method	Precursors and synthesis conditions	Molarity, M	Structure	Crystallite size, [nm]	Band gap, eV	Other parameters
A jet- nebulizer spray pyrolysis [78]	[$Cu(NO_3)_2.3H_2O$] double distilled water; substrate temperature: 400°C; angular distance: 5 cm	0.1 0.2 0.3	CuO thin films are monoclinic crystal phase in nature		2.1 1.9 1.8	average thickness :98, 109, 112 nm; microstrain: 0.0025, 0.0019, 0.0015 dm^{-2}); 5.60301, 3.25719, 1.88748 average conductivity: $9.02{\cdot}10^{-9}$, $2.55{\cdot}10^{-8}$ and $2.75{\cdot}10^{-8}$ S/cm
Spray pyrolysis [76]	($CuCl_2.2H_2O$), inde-ionized water; rate of spray: 5 ml·min^{-1}; substrate temperature: 350°C; annealing temperature: 400°C for 2 h.	0.05 0.1 0.15	monoclinic structure of CuO	10 17 17	No	microstrain 2.71, 1.62, 162; resistivity ρ (Ω·cm): 0.0579, 0.0680, 0.0159; Hall coefficient RH (10^{-2} $cm^3/1°C$): 1.69, 9.51, 34.25.

Continuation **TABLE 2.**

Method	Precursors and synthesis conditions	Molarity, M	Structure	Crystallite size, [nm]	Band gap, eV	Other parameters
Air-pressurized spray pyrolysis [74]	$CuCl_2 \cdot 2H_2O$, distilled; water, rate of spray: 0.014 mL/s, substrate temperature: 300°C, angular distance: 15 cm	0.01 0.02 0.05 0.1 0.2	polycrystalline nature with monoclinic structure of CuO	4.3 10.8 14.1 12.8 14.7	from 1.59 to 1.91	thickness: 17, 25, 67, 160, 467 nm; the disorder values decrease from 0.60 to 0.30 eV
Chemical spray pyrolysis (CSP) technique by spraying [79]	$(Cu(CH_3COO)_2, H_2O)$ compressed purified air was used as the carrier gas (0.4 kg/cm^2); substrate temperature: 350°C; rate of spray: 5 $ml \cdot min^{-1}$; angular distance: 30 cm	0.1 0.15 0.2	amorphous CuO with monoclinic structure	37 nm 52 nm	2.55 2.50	thickness: 1.03,1.54, 1.94 nm; microstrain ($\varepsilon \cdot 10^{-3}$): 0.973, 0.695
Sol–gel spin coating [80]	$Cu(CH_3COO) \cdot H_2O$, polyethylene glycol (PEG, $H(OCH_2CH_2)n \cdot OH$) diethanolamine (DEA, $C_4H_{11}NO_2$)	0.30 0.35 0.40 0.45 0.50	No	grain size: 63.30; 60.36; 73.70 60.74 67.34	1.90 1.80 1.63 1.59 1.51	thickness 302.38, 349.78, 358.56, 517.86, 662.33 nm; resistivity decreases: 12.76 Ω/cm at 0.5 M; conductivity increases: 0.07S/m at 0.5 M

From the literatures, the increase of grain size resulting reduction in grain boundary scattering, which leads to larger electromobility and enhanced conductivity. Hence, the films of higher molarity have low resistivity. On other hand, carrier concentration increased with increasing molarity of precursor solution [78].

3. EFFECT OF ANNEALING TEMPERATURE

Annealing temperature is an important parameter in the elaboration of thin films where the deposition temperature is involved in all mentioned processes its effect on membranes properties has been studied [81, 82]. Overall results suggest that the formation of CuO nanostructures with different shape, size and morphology can be achieved using different annealing temperatures *via* these routes. The improvement in their crystallinity and purification can be further attained by controlling of the temperatures [83].

3.1. Structural Properties

Temperature affects the structural structure of copper oxide films, and this means that its effect is clear on the optical, electrical and morphological properties. It was found in many studies that, by increasing the temperature from room temperature to higher degrees, the phases of the films change. When the Cu_2O thin films are annealed molecular vibrations increases and lattice oscillations cause the weak bonds resulting the break and switch to CuO crystal structure. Figure 3 shows the crystal structure of CuO and Cu_2O. These structures arise as more stable structures because of their strength [84–88]. This

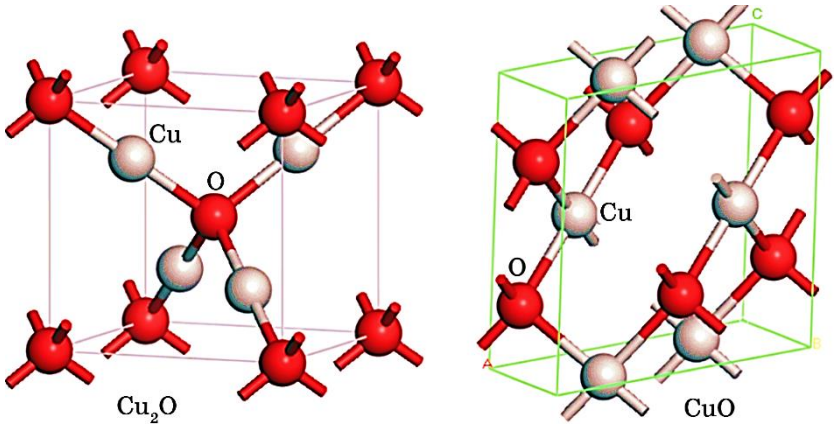

Fig. 3. Crystal structure of CuO and Cu_2O.

means that higher temperature caused significant oxidation of pure copper in air as shown in Eq. (7):

$$4Cu + O_2 \rightarrow 2Cu_2O. \quad (7)$$

Continued increase in temperature leads to further oxidation of Cu nanoparticles (NPs):

$$2Cu_2O + O_2 \rightarrow 4CuO. \quad (8)$$

The oxidation kinetics depends on many factors such as temperature, oxygen partial pressure, annealing time, *etc.* [89].

Observed during formation of a Cu oxide shell (Cu_xO) followed the order Cu_2O, and CuO with increasing temperature. We note that the formation of pure Cu_2O thin films occurs at low temperatures (around 200°C), while the formation of a pure CuO films requires higher temperature ranged from 300 to 500°C. However, the formation of Cu_4O_3 phase mixed with other CuO compounds are rarely [90]. The films deposited at low temperature showed clearly the peaks, which indicate Cu_2O (cuprite) phase corresponding to (111) plan observed at $\cong 2\theta = 36.4°$ [91, 92]. That is the last one becomes unstable at partially converted to CuO (tenorite) represents the mixed phase of copper, which match reflections forms near (111) for CuO and decrease in peak (200) for Cu_2O [93]. Down to the pure phase of CuO (tenorite) with (111) plan positioned at ($\cong 2\theta = 38{,}7°$) and in some cases, $(\bar{1}00)$, is a diffraction peak at 35.4° with a gradual rise in temperature reported by Khojier *et al.* [94]. Figure 4 illustrates XRD patterns of the as-

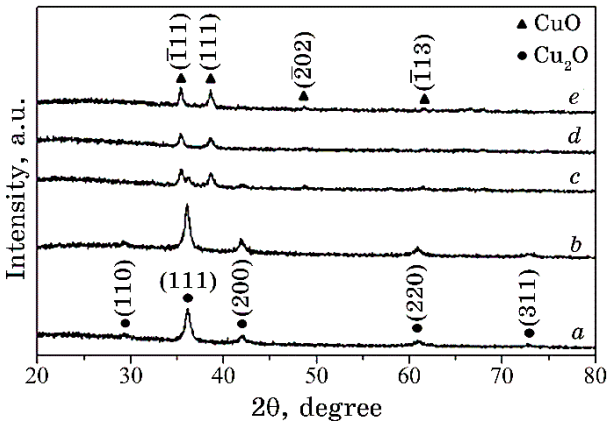

Fig. 4. XRD patterns of copper oxide films: (*a*) the as-deposited film; (*b*) the film annealed at 200°C for 1 h, and the films annealed at 300°C for (*c*) 1; (*d*) 2; and (*e*) 4 h, respectively.

deposited and annealed thin films [95].

However, when the oxidation temperature was higher, the transformations that occur in the membranes from one phase to another do not mean the complete disappearance of the other phases, but only a decrease in their intensity, where the degree to which these changes will occur remains, it depends mainly on the method adopted in the synthesis of the membranes, within the search of the authors, higher annealing temperatures leads to the lattice constants a, b and c decrease [93, 96].

The annealing temperature had an impact on the crystallite size (D); several researchers observed that it was increasing [97]. In spite of that, some exceptions were noted, where the crystallite size decreased [98].

Noteworthiness, Raman spectrometry was used to analyse the phase of the material prepared. The copper (II) oxide phase crystallizes in a tenorite structure (monoclinic crystal system), which is represented by symmetry group $C2/c$ C_{2h}^6 $n\circ 15$. Its Bravais space cell is composed of two-unit formulas; Cu atoms occupy C_i symmetry sites, and O atoms are placed in $C2$ symmetry sites [99, 100]. The metal cation copper forms four coplanar bonds with oxygen, which again self-coordinated by four copper atoms, forming two sets of chains directed along (110) direction [100, 101]. The factor group analysis yields [102]:

$$\text{Cu: } \Gamma = 3A_u + 3B_u; \text{ O: } \Gamma = A_g + 2B_g + A_u + 2B_u.$$

This crystal has 12 degrees of freedom with the following irreducible representation: $4A_u + 5B_u + A_g + 2B_g$, *i.e.*, 3 acoustic modes ($A_u + 2B_u$), 3 Raman activity modes ($A_g + 2B_g$), 6 IR-activity modes ($3A_u + 3B_u$). (Three well know peaks of copper oxide (296, 346, 632) cm^{-1} are assigned to A_g and $2B_g$ CuO phonon peaks [95].)

Cu_2O crystallizes in a cuprite structure (cubic crystal system), represented by symmetry group $Pn3m$ (O_h^4) $n\circ 224$. Its Bravais space cell is composed of two-unit formulas, with Cu atoms occupying $D3d$ symmetry sites, while O atoms are placed in T_d symmetry sites. This crystal has 18 degrees of freedom represented by the following irreducible representation [93]:

$$Cu_2O: A_{2u} + 3T_{1u} + E_u + T_{2u} + T_{2g},$$

where acoustic modes T_{1u}, Raman active modes T_{2g}, infrared (IR) active modes T_{1u}, silent modes $A_{2u} + E_u + T_{2u}$.

B. Balamurugan *et al*. studied Raman spectra of Cu_2O; they reported two relatively strong peaks at 570 cm^{-1} and 618 cm^{-1}. These correspond to the Cu_2O phase [103].

Figure 5 shows Raman spectra of CuO nanostructures at different annealing temperatures.

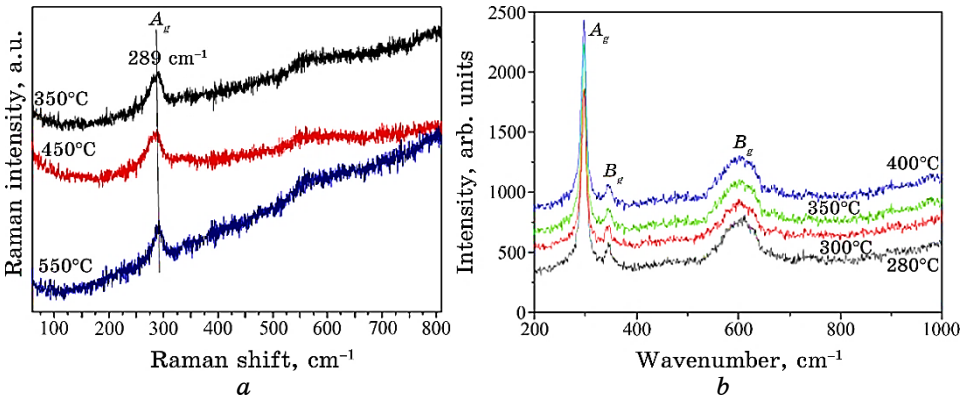

Fig. 5. Raman spectra of CuO thin films at different annealing temperatures: *a*—[104]; *b*—[105].

3.2. Morphological Properties

Generally, in PVD techniques the film formation is achieved through the species condensation on the substrate which resulted that the films deposited by these techniques being more homogenous, denser, and smoother with good adherence.

However, films prepared by CVD techniques are formed through chemical reactions coming from the solution. CuO films deposited by these techniques are generally uniform and have fewer adherents.

The variations in morphology are significantly influenced by the annealing temperature where the change in phases results in a change in the crystal size [106], which increases with the increase in the annealing temperature.

On the other hand, a decrease in dislocation density and microstrain was reported [94, 107]. This increase leads to grain uniformity [88]. Lower surface roughness, and a homogeneous morphological structure as reported [108].

3.3. Optical and Electrical Properties

All works noticed that the decrease in the forbidden band gap (E_g) is likely due to the increase in crystal size and modification of the grain boundary formation during growth. It causes a narrowing of the forbidden band gap, or due to a low concentration of traps near the conduction band [109].

Gopalakrishnan *et al*. reported a decrease in the optical band gap energy from 1.8 to 1.2 eV with increasing substrate temperature from 250–350°C [78].

TABLE 3. Summary on the effect of annealing temperature on the properties of copper oxide.

Method	Parameter	Temperature	Morphology	Structure	Size, [nm]	Band gap, eV	Other parameters
Sol–gel (nebulizer spray pyrolysis) [91]	0.04 M ($C_4H_6O_4.H_2O$), pure glucose ($C_6H_{12}O_6$), 20 vol.% of 2-propanol ($(CH_3)_2$ CHOH)	250°C 280°C 310°C 320°C	nanoparticles — all the films have spherical shaped particles the increase in particle size with the temperature	250(Cu_2O) 280(Cu_2O) 310(Cu_2O) 320(CuO)	20 25 22 33	$4.26{\cdot}10^{-4}$ $8.66{\cdot}10^{-4}$ $1.06{\cdot}10^{-3}$ $2.16{\cdot}10^{-3}$	Hall mobility cm^2/vs: 0.41, 0.55, 0.61,1 strain×10^{-2}: 0.54, 0.430.48, 0.33 (TC): 0.97, 1.29, 1.17, 2.72
The thermal method [23]	copper slides	300°C 400°C 500°C	nanoparticles the temperatures increases, the morphology of the film increases	Cu_2O and Cu CuO CuO	26.763 42.811 47.572	No	transition of Cu from hydrophobicity to hydrophilicity

Continuation **TABLE 3.**

Method	Parameter	Temperature	Morphology	Structure	Size, [nm]	Band gap, eV	Other parameters
A remote plasma sputtering [115]	radiofrequency (RF) launches power 1200 W the target power set at 300 W, pressure: $4.3{\cdot}10^{-3}$ mBar, partial pressure of Ar = $9.0{\cdot}10^{-6}$ mBar	as-deposited	all of the CuO films possess compact nanostructures with very plane and smooth surface	CuO thin films have a monoclinic structure	13	increases from 1.1 to 1.37	the carrier concentration, cm^{-3}: decrease from 4.2 to 5.3. mobility cm^2/vs: increase from 0.8 to 2.3 with increasing of the temperatures
		250°C			14.3		
		350°C			14.8		
		450°C			14.8		
Continuous current electrodeposition [93]	thermal Oxidation of Cu2O samples in electrolyte of $CuSO_4$, deionized water NaOH, Lactic acid, PH = 10	as-deposited	for the Cu_2O sample small round crystallites, nucleation centres for CuO, which grow and coalesce, forming a thick material; the sample presents a homogeneous surface	$Cu_2O{\cdot}Cu_zO$ decrease of Cu_zO and increasing in CuO	increase	2.09 eV for Cu_2O and 0.76 eV for CuO	*p*-type semiconductors
		200°C					
		300°C					
		400°C					

Continuation **TABLE 3.**

Method	Parameter	Temperature	Morphology	Structure	Size, [nm]	Band gap, eV	Other parameters
Heat treatment approach [97]	$(Cu(NO_3)_2.3H_2O)$ and the polyvinyl pyrrolidone deionized water has been used as the solvent	500°C 600°C 700°C 800°C	nanoparticles (particles were quite uniformly spherical in shape and had a tendency to aggregate due to the calcining temperature increment	CuO monoclinic phase	(D by DRX) 9 nm,14 nm, 18 nm, 23 nm respectively (D by TME) 9 ± 2 nm, 15 ± 5 nm, 19 ± 7 nm, 24 ± 7 nm, respectively	2.78 2.66 2.35 2.46	*the FTIR spectra confirmed the presence of metal–oxygen bond of CuO nanoparticles. *the samples exhibited a strong blue emission with a photoluminescence peak at 457 nm and green emission peak at 531 nm while the PL intensities were enhanced with temperature increment and attained their maximum at 800°C
Sol–gel (spin coating) [104]	$2g$ ($CuCl_2$) in 10 ml of (CH_3OH), glycerol ($C_3H_8O_3$), HCl, trimethylamine (C_3H_9N)	350°C 450°C 550°C	homogeneous distribution of spherical shape of the CuO nanoparticles at 350°C and 450°C exhibited uniform and relatively dense surface with a small crystallite size (lower than 100 nm) at 550°C shows a cloud-like structure	CuO CuO CuO	19.99 27.06 31.47	2.40 2.55 2.66	at 450°C CuO films exhibit a relatively high absorption in the visible region ranging from 400 to 800 nm, indicating suitability of the material for the solar cell applications

Continuation **TABLE 3.**

Method	Parameter	Temperature	Morphology	Structure	Size, [nm]	Band gap, eV	Other parameters
SILAR [24]	$CuSO_4$; $5H_2O$, $Na_2S_2O_3$, NaOH 40 immersions cycles at 70°C	as-deposited 70 100 300 500	the film is homogeneously, spherical like particles and little rod-shaped particles; the vacancies between particles; tickles reduced; clusters increased	Cu_2O Cu_2O CuO CuO		2.57 2.52 2.45 1.91	mobility cm^2/Vs: (4.20, 9.42, 20.25, 31.87). resistivity Ω·cm: ($6.12 \cdot 10^4$, $7.44 \cdot 10^3$, $8.23 \cdot 10^3$, $5.11 \cdot 10^2$)
SILAR [116]	($CuCl_2$) 10:1 NH_3	as-grown 200°C 300°C 400°C	CuO thin films have an increased homogeneity, density, and smoothness	CuO thin films have a monoclinic structure.	*D* by DRX 11.09 12.05 13.86 14.88	1.17 1.29 1.30 1.36	surface roughness values decrease (58, 45,37,24) nm, respectively, with increasing of the annealing temperature; results showed that the molecular structure of CuO thin film was positively affected by the annealing temperature of the CuO phase

Continuation **TABLE 3.**

Method	Parameter	Temperature	Morphology	Structure	Size, [nm]	Band gap, eV	Other parameters
Chemical deposition (immersed) [117]	125 ml of 1 M $Na_2S_2O_3$ 25 ml of 1 M ($CuSO_4$; $5H_2O$ Distilled water was added to the solution to form 250 ml stock solution of the metal ion complex in standard volumetric flask	as-deposited	the as-prepared a rough surface and irregular grain size;	all samples are polycrystalline at 200°C: Cu_2O at 300°C, Cu_2O (cuprite) become unstable and partially converted to CuO at 400°C CuO	by DRX increase in average crystallite size from 14 to 26 nm; by SEM at 400°C was around 0.9 µm; grain size increases (from 52.3 µm to 65.5 µm) than (from 65.5 µm to 97.6 µm)	2.4 2.4 2.06 1.73	FTIR spectroscopic measurements further proved that the conversion from copper (II) oxide into copper (I) oxide after annealing the films at 300°C; — PL intensity is greatly improved with the increase in annealing temperature and the photoluminescence stability is also improved after annealing
		200°C	at 200°C: does not changed much but				
		300°C	showed better uniformity in grain size; at 300°C a				
		400°C	continuous and homogeneous granular surface; at 400°C dense spherical structures and no visible defects				

The dependence of the band gap energy on substrate temperature was recorded by different workers. This dependence is attributed to the stress in films deposited at low temperatures, which results in films band gap broadening [89, 104, 110].

As for Urbach energies (E_u), their values are inversely proportional to the band gap energy, and this inverse proportionality is logical because it expresses the disorder of the crystal lattice. Ravichandran *et al.* have observed a decrease in disorder from 533 to 470 meV for as-deposited and for CuO thin films annealed at 450°C, respectively; thin films were deposited by the SILAR method [111]. Mugwanga *et al.* have reported that the values of the disorder are in the range of 60–192 meV for various oxygen influx rates changing from 5 to 22.5 (Sccm) during films growth using the reactive dc magnetron sputtering technique [112].

Increasing the crystallite size reduces the effect of the grain boundaries that act as traps for free carriers and thus increases the life of the carriers, which leads to a decrease in the resistivity, for CuO thin films prepared by the thermal oxidation method. L. De Los Santos Valladares *et al.* have reported resistivity equal to $4.2 \cdot 10^{-2}$ Ω·cm at 150°C which decreased to $1.8 \cdot 10^{-11}$ Ω·cm with increasing the annealing temperature to 1000°C [113], or, in other words, the increase in the conductivity may be due to the increase in the free carriers as a result of the presence of copper atoms in the interstitial positions and the presence of oxygen gaps [105].

We conclude that the annealing temperature is indeed the most important thin film parameter that determines the shape and properties of the film. By increasing the temperature to around 300°C, the film structure can change from a cuprite to a tenorite phase.

The properties of deposited films can be varied and thus controlled by changing the deposition temperature; it influences the structural, optical, and electrical properties of thin films.

4. EFFECT OF THICKNESS

The thickness is an important parameter in the elaboration of thin films, the thicknesses of films, elaborated by different methods at various experimental conditions, was measured by different techniques such as cross-sectional SEM 2*D*-image, profilometer, envelope method based on transmittance measurement.

4.1. Structural Properties

It was found that the thickness affects the properties of the films, where for the thickness is less, it was found that the grains are irregu-

lar and there are many cracks and crystalline gaps, which indicate poor homogeneity of the sample, while it is homogeneous and dense with a smaller surface roughness with increasing thickness [118]. Also, as the thickness of the films increases, the size of the grains increases, and the shape of the grains changes from regular hexagonal to triangular [119].

4.2. Optical Properties

Approaching the infrared spectral zone, the transmittance is reduced with the augmentation of the films thickness. First, this variation may be linked to the structural. Second, the reduction of the transmission may be associated to the thickness increase CuO thin layers reveal a high intrinsic absorption in the visible range and all the transmission spectra exhibit a sharp fall of transmittance at the band edge when the value of the arriving photon energy is above or equal to the gap of the semiconductor [119].

Figure 6 illustrates that the transmittance of the films increases with the increase of the thickness [120]; in this context, L. Chabane has demonstrated that the optical band gap gradually widens as the grain size increases with thickness [121].

4.3. Electrical Properties

The larger grain size results in a lower density of grain boundaries, which behave as traps for free carriers and barriers for carrier transport in the film.

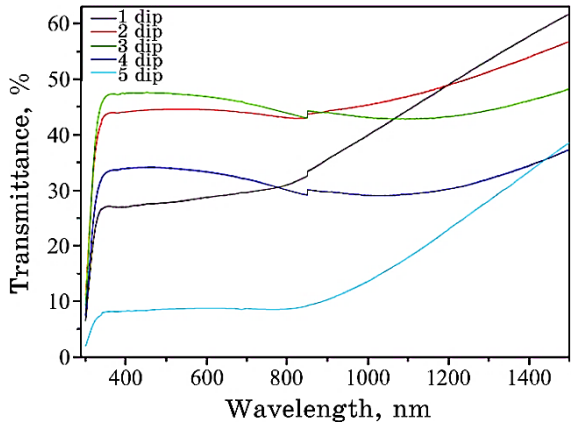

Fig. 6. The optical transmittance spectra of the obtained films of CuO elaborated with various thicknesses.

TABLE 4. Summary on the effect of thickness on the properties of copper oxide.

Method	Precursors and synthesis conditions	Thickness	Structure	Crystallite size, [nm]	Band gap, eV	Other parameters
Spray pyrolysis technique [119]	$CuCl_2$, $2H_2O$ de-ionized water a nozzle positioned: 28 cm, flow rate: 3 $ml \cdot min^{-1}$, substrate temperature: 300°C	180 450 970 1730 1950 2270 2900	monoclinic crystal structure and tenorite phase	24.9 62.4 38.7 50.3 50.3 71.9 55.9	1.63 1.63 1.58 1.56 1.53 1.52 1.52	the strain increase (–0.084, –0.053, 0.208, 0.161, 0.148, 0.204, 0.127), respectively; resistivity 94.26, 65.37, 43.41, 8.51, 24.7 Ω·cm, Hall mobility 2.19, 14.67, 22.44, 54.56, 34.13 $cm^2 \cdot V^{-1} \cdot s^{-1}$ for 940, 1730, 1950, 2270, 2900 nm, respectively
Dip-Coating technique [120]	$CuCl_2$, $2H_2O$ in CH_3OH, withdrawal speed: 1330 µm/s. annealing temperature: 500°C for 1 h	471.04 556.64 764.61 834.01 1219.36	single phase CuO with monoclinic crystal; the intensity of the peaks is significantly increasing with increasing of the thickness	30.72 29.34 27.57 26.58 27.75	3.80 3.86 3.88 3.82 3.70	the strain 0.1139, 4.4413, 4.7321, 0.1382, 0.1282, respectively; the resistivity increases with increasing in the thickness and its values are in the range of tens to hundreds of Ω·cm

Continuation **TABLE 4.**

Method	Precursors and synthesis conditions	Thickness	Structure	Crystallite size, [nm]	Band gap, eV	Other parameters
Thermal evaporation technique [124]	coating unit in vacuum $3.2{\cdot}10^{-5}$ mbar. the distance between the boat and substrate: 18 cm, temperature: 300°C for 1 h	250 300 350 400	polycrystalline in nature; the monoclinic structure	14.65 14.70 16.24 19.39	they were found to be in the range of (1.6 to 11 1.3) eV when the film thickness varying from 250 to 400 nm	roughness 0.645, 0.878, 1.09, 1.01 average grain size 67.38, 74.34, 79.44, 83.20
Ultrasonic spray pyrolysis [125]	$CuCl_2$ in be-distilled water; the arriving liquid is atomized by 40 kHz ultrasonic, temperature: 300°C distance nozzle substrate: 4 cm	429 612 852 1020	No	17.24 21.31 24.02 26.22	No	decrease of the resistivity from 1329 Ω·cm to 9.123 Ω·cm with the increasing of the thickness

Hence, an increase in the grain size can cause a decrease in grain boundary scattering, which leads to an increase in the conductivity. Thus, the initial decrease in resistivity and this, what is reported by S. S. Shariffudin *et al.* [122] and [79], is due to an increase in both carrier density and carrier mobility of the films, which result from the increased grain the resistivity can be related to the increase in carrier scattering due to a decrease in grain size or to other discontinuities of the film size. The influence of crystallite size on activation energy was studied extensively [123].

We conclude that thickness has a role on degree of crystal orientation; it is closely attached to some of the other parameters. So, it increases with molarity [74, 72], number of dips [120] deposition time [125, 126], and annealing temperature [127]. Whereas, decrease with increase of spin-coating speed and of dip coating drawls speed [122].

Besides preparation factors, physical properties of CuO films can also be altered by addition of dopants. Doping, in general, is a powerful technique for optimizing the sensing properties of metal oxide semiconductors.

From the literature, the use of extrinsic elements on CuO has been widely. Where, the presence of impurity at the interfaces, vacancy, vacancy cluster at the grain and grain boundaries can play an important role on the materials behaviour. These defects offer a scope to tune the useful material properties in order to improve it. It is well known that interstitial oxygen O_i and free copper V_{Cu} are determined as the acceptors in CuO, and that these acceptors can take the place of lattice defects and atomic impurities.

In this regard, various elements of large and small radius such as lanthanide ions (La^{3+}, Ce^{3+}, Pr^{3+}, Sm^{3+}, Nd^{3+}, Gd^{3+}, Tb^{3+}, Dy^{3+}) [128–132], transition metals (Mn^{2+}, Cd^{2+}, Zn^{2+}, Ni^{2+}, Fe^{3+},Y^{3+}, Cr^{2+}, Pd^{2+}, Ag^{+}, Ti^{4+}) [133–139], post-transition metals (Al^{3+}, Ga^{3+} and In) [140–142], semimetals (Sn^{3+}, Pb^{3+}) [143, 144], and alkali metals (Li^{+}, Na^{+}, and K^{+}) [145] are incorporated into CuO lattice for different applications as ferromagnetic oxide, conductivity improvements or photocatalytic properties. In this part, we review the most important studies related to the dopant effect on the performance of films and their applications.

Theoretically, *p*-type doping in CuO may be possible by substituting any group I elements (Li, Na, and K) as alkali metals acting as surface acceptors in Cu sites; group I elements might be better *p*-type dopants elements at shallow acceptor levels. However, experience has shown that group I elements tend to occupy interstitial locations, because of their small atomic radii, rather than substitution locations; so, they act as donors instead of acceptors.

By H. Siddiqui *et al.*, high-quality pristine CuO- and Na-doped CuO nanostructures were made using a sol–gel method, with doping values of 1.0, 3.0, 5.0, and 7.0 mol.% CuO/Na. The XRD analysis reveal the

structural alteration from monoclinic to cubic symmetry with increase in doping level and also reveal the phase purity up to 3% doping level, and beyond this (*i.e.*, for 5 and 7% doping level) the involvement of Na_2O phase increases with increase in Na concentration in CuO/Na system. Morphology of the samples indicates that the Na-doped CuO nanostructures exhibit less agglomeration compared to pristine CuO nanoparticles. Moreover, from the diffused reflectance spectrum, it is inferred that CuO/Na nanoparticles exhibit a microstructural defects and ionic impurities, which play an important role in modifying its band gap. The observed shift in band gaps 1.49 eV undoped CuO (1.48, 1.46, 1.51, 1.53) with increasing doping level is attributed to the nanosize effect as well as to the Cu_i and O_i-defects, which gives high conducting behaviour of Na-doped CuO nanoparticles [146].

V. T. Trang *et al.* concluded that potassium ion (K^+) doping has ability to improved electrochemical performance. The optimized K^+-doped CuO nanostructure $K_\chi Cu_{1-\chi}O_{1-\delta}$ ($\chi = 0.10$) was synthesized using a solvothermal method followed by annealing at 500°C for 5 h under air atmosphere. The morphology of CuO was slightly changed by the doping of K^+-ions in comparison to undoped CuO. X-ray diffraction analysis demonstrates that the K^+-ion doping caused no change in the phase structure in the doped sample, the CuO nanoparticle size is in the range of 25–50 nm, whereas the undoped CuO nanoparticles show a range of 50–100 nm with large agglomeration. On the other hand, the K^+-doped CuO nanoparticle electrode exhibited a high specific capacity of 354.6 $mA{\cdot}h{\cdot}g^{-1}$ at 0.1 C after 30 cycles, but in spite of this, it also retained 162.3 $mA{\cdot}h{\cdot}g^{-1}$ at a high current rate of 3.2 C, which is much higher than that of undoped CuO (only 68.9 $mA{\cdot}h{\cdot}g^{-1}$ at 3.2 C). The present study will be beneficial to the development of high-capacity and long-cycling-life anode materials for the next generation of Li-ion cells [147].

C. Y. Chiang *et al.* were studied Li doped CuO nanoparticles prepared by flame spray pyrolysis and followed by spin coating where synthesized at dopant concentrations of 0.5 at.%, 2 at.%, 3.5 at.% and 5 at.%, they found that The photocurrent density and photon-to-hydrogen conversion efficiency increased by a factor of five to ten when introducing Li into CuO, and they justified this to the increase in the electrical conductivity of the film by almost two orders of magnitude, *i.e.*, from $2{\cdot}10^{-6}$–$4{\cdot}10^{-6}$ S/cm to $7{\cdot}10^{-5}$–$3{\cdot}10^{-4}$ S/cm, and thus, the increase in the lifetime of the photogenerated charge carriers. The best they got it photocurrent density and photon-to-hydrogen conversion efficiency was 1.69 mA/cm^2 and 1.3%, respectively, corresponding to the film prepared by 2.0 at % Li–CuO sintered at 450°C for 1 h with the thickness 1.7 μm at bias voltage of –0.55 V *vs.* Ag/AgCl in 1M KOH and under 1 sun illumination [148].

Another study by F. Z. Chafi *et al.* has reported that the incorpora-

tion of metal ions such as Fe^{3+}, can contribute to more oxygen defects on CuO along with an increase in the charge density of CuO, which subsequently can induce higher performance of the nanostructure. Hence, higher conductivity increased from 0.138 to 15.0873 as Fe dopant concentration advances, oxygen vacancies also reduce the activation energy that facilitates the sensor device to respond at low temperatures. From the temperature dependent sensing measurements, it is found that for all samples, the sensing response increases with temperature up to 75°C beyond which decreases due to the desorption of oxygen at the sensor surface. At room temperature, the sensor response was found to have a power law dependent relation [149].

As mentioned in one of the articles they used ion of rare earth as doping in copper oxide. Vimala Devil *et al.* proposed the use of ions La it was prepared by solution combustion method and subsequent annealing at different temperatures, which the presence of La ion in CuO showed a peak shift in XRD pattern and a significant and work to reduce the crystallite size and induces more number of non-radiative transition centres in CuO. Annealed samples led to the growth of aggregated spherical shaped morphology. PALS studies clearly denote the presence of vacancies, cluster vacancies and microvoids in CuO and La-doped CuO. The presence of defects is revealed from the three lifetime components. The decrease in their values upon annealing showed the recovery of Cu vacancy type defect, reduced cluster vacancies and microvoids in pure and doped CuO. Incorporation of La ion in CuO lattice increased the lifetimes compared to undoped CuO. Annealed CuO sample at 800°C, exhibited a shortest lifetime of 137 ps with a significant reduced lifetime of 121 ps for La-doped CuO. The increased τ_{av} and *S* value of La-doped CuO with that of undoped CuO denotes the presence of more number of defects in doped samples. The photoluminescence spectra clearly inferred the increased intensity in defect related peaks due to doping and annealing without the shift in the peak position. It is mainly due to the lattice mismatch and difference in oxidation state between Cu^{2+} and La^{3+} ion in correlation with positron studies. The defects in La-doped CuO induced more number of quenching sites for non-radiative transition. The increase in concentration of defects in La-doped CuO is well supported by the lifetime and Doppler broadening measurements. The presence of defects is quantitatively and qualitatively explained using positron and PL studies [150].

S. Bhuvaneshwari *et al.* uniform copper oxide nanoboats undoped CuO nanorods, (NRs) and Cr doped (2 at.% and 6 at.%). CuO nanoboats (NBs) have synthesized by a low-temperature hydrothermal route for a room-temperature NH_3 sensing prototype application with an enhanced sensitivity. They were observed in PL emission spectra; a strong green emission at 566 nm validates the increase in oxygen vacancies, which, in turn, boost the sensing response by adsorbing more

surface oxygen increase in with the gas concentration.

Among the three CuO samples, 6 at.% Cr-doped CuO nanoboats showed a 2.5-fold increase in sensor response observed at room temperature and a maximum sensitivity of 180% at 75°C for 600 ppm of NH_3 that is better than NH_3 sensitivity, which is attributed to the higher specific area at the surface and oxygen vacancies which is not evident in undoped CuO nanorods [151].

In this work, has endeavoured to demonstrate that Ag-doped CuO has a greater specific surface area of nanoparticles and greater lattice deficiency. Moreover, the transparency is reduced with increased silver content [152]. The transparent Ag-doped CuO may offer potential applications in areas of photocatalysis, electronics, and optics. In similar work by J. Huang *et al.* is to report the using of Ag to doping the electrode of array of CuO nanosheet *via* the silver mirror reaction. The Ag loaded on the CuO nanosheet arrays improved the electrical conductivity of the electrode and also enhanced the electrical contact among the substrate the active materials and the electrolyte, resulting in lower polarization with higher electrochemical activity.

The specific capacitance of the Ag-doped CuO nanosheet electrode is 689 Fg^{-1} at $1Ag^{-1}$ and 299 Fg^{-1} at $10Ag^{-1}$, respectively, much higher than that of the unmodified CuO nanosheet arrays (418 Fg^{-1} at 1 Ag^{-1} and 127 Fg^{-1} at 10 Ag^{-1}). The improved capacitance is explained in terms of the presence of dispersed Ag particle coated. The results show that the thickness of a single nanosheet is up to around 150 nm.

Due to considering the low cost, abundance resource and the high specific capacitance, the NSA–Ag/CuO electrode has the promise as potential electrode materials for pseudo-supercapacitors [153].

Saeid Masudy-Panah *et al.* The present work provides a possible solution for the growth of doped CuO for photovoltaic application. The potential of Ti to serve as a useful dopant in CuO thin film was investigated. It was shown that the Ti content in the deposited films could be controlled by tuning the sputtering power during the film deposition. They have undoped and four different concentration: 0.049 at.%, 0.099 at.%, 0.19 at.%, 0.598 at.% Ti. Microstructural analysis revealed that the crystal quality of samples was not significantly influenced when the Ti content was increased up to 0.099 at.%. By tuning the Ti doping, it was found that it is possible to improve the conductivity of the deposited thin films, while retaining the optical properties and crystal quality. The *p*-CuO (Ti)/*n*-Si heterojunction solar cells fabricated using Ti-doped CuO absorber layer exhibited improved solar cell parameters compared with undoped cells [139].

S. N. Vidhya *et al.* demonstrated that CuO thin films doped by Ga have morphological and optical properties and it confirms the suitability of these films for photocatalytic and optoelectronic applications for that the spray pyrolysis method was used to create the conductive pure

and Ga-doped copper oxide thin films. X-ray diffraction studies confirm that all the films are in polycrystalline nature for Ga-doped CuO. A good surface morphology was revealed by SEM studies for both pure and Ga-doped films. The grains are uniformly distributed over the entire scanned surface without any patches for concentrated 2 ml Ga-doping. The surface is found to be smooth without any undulation. A variation in the average transmittance, which is about 60–70% for the Ga-doped CuO films and the maximum band gap value of 2.24 eV is obtained for the 2 ml Ga-doped CuO [154].

By A. Yildiz *et al.*, this work is describes hopping conduction in In–CuO using dip-coating route for manufacture of the layers and they used three concentrations 1%, 5%, 10%, the crystallite size was calculated and given 19, 17, 8 and 10 nm for undoped, 1% In, 5% In and 10% In doped samples. Furthermore, the band gap is increasing from 1.24 to 1.46 eV with the increasing doping level.

The resistivity of the films was characterized by the Mott VRH model for 160 K < T < 300 K, while it exhibited a metallic-like behaviour for T < 160 K. The complete set of parameters describing the properties of the carriers (the hopping distance and the value of the density of states at the Fermi level) was determined. The temperature dependent resistivity data of the films were well explained by fluctuations in these parameter [142].

However, that over-doping could attribute to the reduction of CuO efficiency. This is probably due to the excess dopants that act as trapping sites for both electrons and holes and this was hence proved by Jing Wu *et al.*, when they proposed the so–gel technique to prepared Sn:CuO films with different Sn concentrations (0.5, 1, 1.5, 2) in order to study the influence of Sn doping on the structural, optical and electrical properties of Sn:CuO films. The results showed the Hall mobility and resistivity reduced: 19, 10.5, 7.58, 6.18, 7.14 cm^2/Vs, 64.8, 54.7, 47.4, 77.5 ($\Omega \cdot cm$), respectively [155].

F. Bayansal *et al.* presented the first report on the morphological, structural and optical properties of Pb-doped CuO nanostructured thin films were studied at dopant concentrations of 0.27 ,0.36, 0.37, 0.46, 0.75 at.% and were synthesized by the successive ionic layer adsorption and reaction method. The results showed them that the morphology of the film surface was changed from plate-like to coral-like nanostructures with increasing Pb concentration. The x-ray diffraction patterns showed the monoclinic crystal structure with preferential planes of (111) and (111). Furthermore, ultraviolet–visible spectra showed that the band gap of the films was illustrated 1.43, 1.80, 1.76, 1.72, 1.68, 1.65 eV with increasing of the concentration [156].

It can be said that methods like CuO coupling with other dopants will improve their performance by producing smaller particles with high specific surface area, shifting the band gap energy, suppressing the

rate of electron–hole pair recombination, increasing charge separation efficiency, and enabling better dispersion in the medium.

5. CONCLUSIONS

We took the research on a tour d'horizon of different aspects of copper oxide, starting from the fundamentals of synthesis to its properties that express the appropriate promising application; we focused on some factors along with the routes of synthesizing process for CuO nanostructures. what we can say already is that accurate control of synthetic strategies is very important since it makes it possible to obtain CuO nanostructures with manageable dimensions and morphology.

In order to provide greater stability and better performance, future research should seek to overcome the disadvantages of CuO and the practical problems that still exist.

REFERENCES

1. A. J. Resende, *Copper-Based p-Type Semiconducting Oxides (from Materials to Devices* (Université Grenoble Alpes–Univ of Liège: 2017) (in French).
2. B. K. Meyer, A. Polity, D. Reppin, M. Becker, P. Hering, P. J. Klar, Th. Sander, C. Reindl, J. Benz, M. Eickhoff, C. Heiliger, M. Heinemann, J. Bläsing, A. Krost, S. Shokovets, and C. Müller, and C. Ronning, *physica status solidi (b)*, **249**, Iss. 8: 487 (2012); https://doi.org/10.1002/pssb.201248128
3. T. Mahalingam, J. Chitra, J. Chu, S. Velumani, and P. Sebastian, *Solar Energy Materials and Solar Cells*, **88**, Iss. 2: 209 (2005); https://doi.org/10.1016/j.solmat.2004.05.026
4. P. R. Markworth, X. Liu, J. Y. Dai, W. Fan, T. J. Marks, R. P. H. Chang, *Journal of Materials Research*, **16**, Iss. 8: 2408 (2001).
5. P. Mitra, *Journal of Physical Sciences*,**14**: 235 (2010).
6. A. Y. Oral, E. Menşur, M. H. Aslan, and Engin Başaran, *Materials Chemistry and Physics*, **83**, Iss. 1: 140 (2004); https://doi.org/10.1016/j.matchemphys.2003.09.015
7. A. Ogwu, T. Darma, and E. Bouquerel, *Journal of Achievements in Materials and Manufacturing Engineering*, **24**, Iss. 1: 172 (2007).
8. M. Al-Kuhaili, *Vacuum*, **82**, Iss. 6: 623, (2008); https://doi.org/10.1016/j.vacuum.2007.10.004
9. K. Santra, C. Sarkar, M. Mukherjee, and B. Ghosh, *Thin Solid Films*, **213**, Iss. 2: 226 (1992); https://doi.org/10.1016/0040-6090(92)90286-K
10. N. Silva, S. Ramírez, I. Díaz, A. Garcia, and N. Hassan, *Materials*, **12**, Iss. 5: 804 (2019); https://doi.org/10.3390/ma12050804
11. S. Mosleh, M.R. Rahimi, M. Ghaedi, K. Dashtian, and S. Hajati, *Ultrasonics Sonochemistry*, **40**: 601 (2018); https://doi.org/10.1016/j.ultsonch.2017.08.007
12. E. Mousali and M. A. Zanjanchi, *Journal of Solid State Electrochemistry*, **23**,

Iss. 3: 925 (2019); https://doi.org/10.1007/s10008-019-04194-9
13. H. Abbasian, D. Ghanbari, and G. Nabiyouni, *Journal of Nanostructures*, **3**, Iss. 4: 429 (2013); https://doi.10.7508/JNS.2013.04.007
14. V.V. Khedekar and B. M. Bhanage, *Journal of the Electrochemical Society*, **163**, Iss. 6: B248 (2016); https://doi.10.1149/2.1101606jes
15. S. Bhuvaneshwari and N. Gopalakrishnan, *Journal of Colloid and Interface Science*, **480**: 76 (2016); https://doi.org/10.1016/j.jcis.2016.07.004
16. M. S. Araújo, R. R. Silva, G. Pacheco, W. R. Lustri, A. Tercjak, J. Gutierrez, J. R. S. Júnior, F. H. C. Azevedo, G. S. Figuêredo, M. L. Vega, S. J. L. Ribeiro, and H. S. Barud, *Carbohydrate Polymers*, **179**: 341 (2018); https://doi.org/10.1016/j.carbpol.2017.09.081
17. Z. Zhong, V. Ng, J. Luo, S.-P. Teh, J. Teo, and A. Gedanken, *Langmuir*, **23**, Iss. 11: 5971 (2007).
18. J. Zhang, J. Wang, Y. Fu, B. Zhang, and Z. Xie, *RSC Advances*, **5**, Iss. 36: 28786 (2015); https://doi.10.1039/C5CP02150B
19. M. A. Choudhary, R. Manan, M. Aslam Mirza, H. Rashid Khan, S. Qayyum, and Z. Ahmed, *Int. J. Mater. Sci. Eng.*, **4**, Iss. 1: 1 (2018).
20. E. Souza, R. Landers, L. Cardoso, T. G. Cruz, M. Tabacniks, and A. Gorenstein, *Journal of Power Sources*, **155**, Iss. 2: 358 (2006); https://doi.org/10.1016/j.jpowsour.2005.04.014
21. J. Kampmann, S. Betzler, H. Hajiyani, S. Häringer, M. Beetz, T. Harzer, J. Kraus, B. V. Lotsch, C. Scheu, R. Pentcheva, D. Fattakhova-Rohlfing, and T. Bein, *Nanoscale*, **12**, Iss. 14: 7766 (2020); https://doi.10.1039/D0NJ05788F
22. R. Wu, Z. Ma, Z. Gu, and Y. Yang, *2010 International Conference on Mechanic Automation and Control Engineering* (2010), p. 3183; https://doi.10.1109/MACE.2010.5535652
23. N. Al Armouzi, G. El Hallani, A. Liba, M. Zekraoui, H. S. Hilal, N. Kouider, and M. Mabrouki, *Materials Research Express*, **6**, Iss. 11: 116405 (2019); https://doi.10.1088/2053-1591/ab44f3
24. C. Mrabet, R. Jaballah, N. Mahdhi, A. Boukhachem, and M. Amlouk, *Journal of Alloys and Compounds*, **968**: 172252 (2023); https://doi.org/10.1016/j.jallcom.2023.172252
25. A. A. Radhakrishnan and B. B. Beena, *Indian J. Adv. Chem. Sci.*, **2**, Iss. 2: 158 (2014).
26. H. Zhu, D. Han, Z. Meng, D. Wu, and C. Zhang, *Nanoscale Research Letters*, **6**: 1 (2011); https://doi.org/10.1186/1556-276X-6-181
27. J. V. Bruckner, S. S. Anand, and D. A. Warren, *Casarette and Doull's Toxicology: The Basic Science of Poison* (Ed. C. D. Klaassen) (2008), p. 981–1051.
28. R. Aelion, A. Loebel, and F. Eirich, *The Hydrolysis and Polycondensation of Tetra Alkoxysilanes, Recueil des Travaux Chimiques des Pays-Bas*, **69**, Iss. 1: 61 (1950); https://doi.org/10.1002/recl.19500690109
29. T. H. Tran and V. T. Nguyen, *International Scholarly Research Notices*, **2014**: Article ID 856592 (2014); http://dx.doi.org/10.1155/2014/856592
30. M. Z.-C. Hu, E. A. Payzant, and C. H. Byers, *Journal of Colloid and Interface Science*, **222**, Iss. 1: 20 (2000); https://doi.org/10.1006/jcis.1999.6610
31. U. T. Khatoon, K. Mohan Mantravadi, and G. Nageswara Rao, *Materials Science and Technology*, **34**, Iss. 18: 2214 (2018); https://doi.org/10.1080/02670836.2018.1482600

32. A. Kahru and H. C. Dubourguier, *Toxicology*, **269**, Iss. 2–3: 105 (2010); https://doi.org/10.1016/j.tox.2009.08.016
33. P. C. Y. Ng, B. J. Long, W. T. Davis, D. J. Sessions, and A. Koyfman, *Internal and Emergency Medicine*, **13**: 375 (2018); https://doi.org/10.1007/-018-1799-9
34. T. Munekata, T. Suzuki, S. Yamakawa, and R. Asahi, *Physical Review E*, **88**, Iss. 5: 052314 (2013); https://doi.org/10.1103/PhysRevE.88.052314
35. D. B. Potter, I. P. Parkin, and C. J. Carmalt, *RSC Advances*, **8**, Iss. 58: 33164 (2018); https://doi.10.1039/C8RA06417B
36. X.-D. Yang, L.-L. Jiang, C.-J. Mao, H.-L. Niu, J.-M. Song, and S.-Y. Zhang, *Materials Letters*, **115**: 121 (2014); https://doi.org/10.1016/j.matlet.2013.10.037
37. L. Guo, F. Tong, H. Liu, H. Yang, and J. Li, *Materials Letters*, **71**: 32 (2012); https://doi.org/10.1016/j.matlet.2011.11.105
38. J. Zhu, H. Bi, Y. Wang, X. Wang, X. Yang, and L. Lu, *Materials Letters*, **61**, Iss. 30: 5236 (2007); https://doi.org/10.1016/j.matlet.2007.04.037
39. J. Zhu, H. Bi, Y. Wang, X. Wang, X. Yang, and L. Lu, *Materials Letters*, **61**, Iss. 30: 5236 (2007); https://doi.org/10.1016/j.matlet.2007.04.037
40. Z. Cheng, J. Xu, H. Zhong, X. Chu, and J. Song, *Materials Letters*, **65**, Iss. 13: 2047 (2011); https://doi.org/10.1016/j.matlet.2011.04.021
41. A. Rydosz, *Coatings*, **8**, Iss. 12: 425 (2018); https://doi.org/10.3390/coatings8120425
42. H. Siddiqui, M. R. Parra, and F. Z. Haque, *Journal of Sol–Gel Science and Technology*, **87**: 125 (2018); https://doi.org/10.1007/s10971-018-4663-5
43. J. Wang, Y. Qi, Z. Zhi, J. Guo, M. Li, and Y. Zhang, *Smart Materials and Structures*, **16**, Iss. 6: 2673 (2007); https://doi.1088/0964-1726/16/6/072
44. *Handbook of Microemulsion Science and Technology* (Eds. P. Kumar and K. L. Mittal) (New York, D.C.: US Govt. Printing Office–Marcel Dekker–CRC Press: 1999); https://doi.org/10.1201/9780203752739
45. P. Mallick and S. Sahu, *Nanoscience and Nanotechnology*, **2**, Iss. 3: 71 (2012); https://doi.10.5923/j.nn.20120203.05
46. A. Sawaby, M. S. Selim, S. Y. Marzouk, M. A. Mostafa, and A. Hosny, *Physica B: Condensed Matter*, **405**, Iss. 16: 3412 (2010); https://doi.org/10.1016/j.physb.2010.05.015
47. N. Zayyoun, B. Jaber, L. Lавnab, E. Ntsoenzok, and R. Bekkari, *J. Mater. Environ. Sci.*, **7**, Iss. 5: 1791 (2016).
48. H. Serrar, A. Bouabellou, Y. Bouachiba, A. Taabouche, A. Bouhank, Y. Bellal, and H. Merabti, *Am. J. Mater. Synth. Process*, **3**, Iss. 2: 12 (2018); https://doi.10.11648/j.ajmsp.20180302.12
49. H. Serrar, A. Bouabellou, Y. Bouachiba, A. Taabouche, A. Bouhank, Y. Bellal, and H. Merabti, *Thin Solid Films*, **686**: 137282 (2019); https://doi.org/10.1016/j.tsf.2019.05.001
50. Zaid Hamid Mahmoud, Nuha Farhan Abdul Kareem, and Aklas Ahmed Abdul Kareem, *Asian J. Chem.*, **30**: Iss. 1: 223 (2018); https://doi.org/10.14233/ajchem.2018.21047
51. E. Benrezgua, B. Deghfel, Z. Abdelhalim, W. J. Basirun, R. Amari, A. Boukhari, M. K. Yaakob, S. Kheawhom, and A. A. Mohamad, *Journal of Molecular Structure*, **1267**: 133639 (2022); https://doi.org/10.1016/j.molstruc.2022.133639
52. L. Znaidi, *Materials Science and Engineering: B*, **174**, Iss. 1–3: 18 (2010);

https://doi.org/10.1016/j.mseb.2010.07.001
53. D. Halin, I. Talib, A. Daud, and M. Hamid, *International Journal of Photoenergy*, **2014**: Article ID 352156 (2014); https://doi.org/10.1155/2014/352156
54. P. Samarasekara and N. Premasiri, *arXiv preprint arXiv*: 1806.03976 (2018); https://doi.org/10.48550/arXiv.1806.03976
55. T. Jiang, Y. Wang, D. Meng, X. Wu, J. Wang, and J. Chen, *Applied Surface Science*, **311**: 602 (2014); https://doi.org/10.1016/j.apsusc.2014.05.116
56. *Indian Institute of Metals, Vol. **21*** (1968).
57. O. Reyes, D. Maldonado, J. Escorcia-García, and P. Sebastian, *Journal of Materials Science: Materials in Electronics*, **29**: 15535 (2018); https://doi.org/10.1007/s10854-018-9110-4
58. S. Farhad, S. Majumder, M. A. Hossain, N. Tanvir, R. Akter, and M. A. Patwary, *MRS Advances*, **4**, Iss. 16: 937 (2019); https://doi.org/10.1557/adv.2019.139
59. V. Avrutin, N. Izyumskaya, and H. Morkoç, *Superlattices and Microstructures*, **49**, Iss. 4: 337 (2011); https://doi.org/10.1016/j.spmi.2010.12.011
60. A. Rakhshani, A. Al-Jassar, and J. Varghese, *Thin Solid Films*, **148**, Iss. 2: 191 (1987); https://doi.org/10.1016/0040-6090(87)90157-X
61. L. Olsen, F. Addis, and W. Miller, *Solar Cells*, **73**: 247 (1982); https://doi.org/10.1016/0379-6787(82)90050-3
62. G. Sığırcık and T. Tüken, *Journal of Materials Science: Materials in Electronics*, **31**: 17855 (2020); https://doi.org/10.1007/s10854-020-04339-x
63. Z. N. Kayani, W. Chaudhry, R. Sagheer, S. Riaz, and S. Naseem, *Materials Science and Engineering: B*, **283**: 115799 (2022); https://doi.org/10.1016/j.mseb.2022.115799
64. A. Maini and M. Shah, *International Journal of Ceramic Engineering & Science*, **3**, Iss. 4: 192 (2021); https://doi.org/10.1002/ces2.10097
65. K. Iimura, Y. Ishikawa, T. Kikuchi, T. Takai, H. Satone, and M. Suzuki, *Journal of the Ceramic Society of Japan*, **125**, Iss. 8: 634 (2017); https://doi.org/10.2109/jcersj2.17012
66. T. Fujiwara, T. Nakaue, and M. Yoshimura, *Solid State Ionics*, **175**, Iss. 1–4: 541 (2004); https://doi.org/10.1016/j.ssi.2004.01.081
67. Q. Zhu, Y. Zhang, J. Wang, F. Zhou, and P. K. Chu, *Journal of Materials Science & Technology*, **27**, Iss. 4: 289 (2011); https://doi.org/10.1016/S1005-0302(11)60064-9
68. T. Karthik, A. Hernández, Y. Kudriavtsev, H. Gymez-Pozos, M. Ramírez-Cruz, L. Martínez-Ayala, and A. Escobosa-Echvarria, *Journal of Materials Science: Materials in Electronics*, **31**: 7470 (2020); https://doi.org/10.1007/s10854-020-02987-7
69. S. Benramache and B. Benhaoua, *Open Physics*, **14**, Iss. 1: 714 (2016); https://doi.org/10.1515/phys-2016-0080
70. S. Joishy, S. D. Kulkarni, R. Choudary, S. R. Maidur, P. S. Patil, and B. Rajendra, *Materials Research Express*, **6**, Iss. 10: 106447 (2019); https://doi.10.1088/2053-1591/ab4153
71. S. Kaur and M. Deshwal, *Transactions on Electrical and Electronic Materials*, **20**, Iss. 4: 309 (2019); https://doi.org/10.1007/s42341-019-00113-x
72. M. Dhaouadi, M. Jlassi, I. Sta, I. B. Miled, G. Mousdis, M. Kompitsas, and W. Dimassi, *Am. J. Phys. Appl.*, **6**, Iss. 2: 43 (2018); https://doi.10.11648/j.ajpa.20180602.13

73. S. Alghamdi, A. O. M. Alzahrani, and M. Aida, *Journal of Optics*, **52**, Iss. 2: 803 (2023); https://doi.org/10.1007/s12596-022-01001-z
74. C. Abdelmounaım, Z. Amara, A. Maha, and D. Mustapha, *Materials Science in Semiconductor Processing*, **43**: 214 (2016); https://doi.org/10.1016/j.mssp.2015.12.019
75. C. Ravi Dhas, Dinu Alexander, A. Jennifer Christy, K. Jeyadheepan, A. Moses Ezhil Raj, and C. Sanjeevi Raja, *Asian Journal of Applied Sciences*, **7**, Iss. 8: 67 (2014); https://doi.org/10.3923/ajaps.2014.671.684
76. A. S. Kumar, K. Perumal, and P. Thirunavukkarasu, *Optoelec. Advan. Mater. — Rapid Commun.*, **4**, Iss. 6: 831 (2010).
77. V. Jagadeesan and V. Subramaniam, *Journal of Materials Science: Materials in Electronics*, **30**: 1571 (2019); https://doi.org/10.1007/s10854-018-0428-8
78. D. Gopalakrishna, K. Vijayalakshmi, and C. Ravidhas, *Ceramics International*, **39**, Iss.7: 7685, (2013); https://doi.org/10.1016/j.ceramint.2013.03.021
79. R. Shabu, A. M. E. Raj, C. Sanjeeviraja, and C. Ravidhas, *Materials Research Bulletin*, **68**: 1 (2015); https://doi.org/10.1016/j.materresbull.2015.03.016
80. H. Hashim, S. S. Shariffudin, M. S. P. Sarah, and N. I. Nasir, *2016 IEEE International Conference on Semiconductor Electronics (ICSE) (17–19 August 2016)* (IEEE: 2016), p. 224; doi:10.1109/SMELEC.2016.7573632
81. M. Yurddaskal, T. Dikici, and E. Celik, *Ceramics International*, **42**, Iss. 15: 17749 (2016); https://doi.org/10.1016/j.ceramint.2016.08.102
82. A. Hassanien, A. Atta, M. El-Nahass, S. I. Ahmed, A. A. Shaltout, A. M. Al-Baradi, A. Alodhayb, and A. Kamal, *Optical and Quantum Electronics*, **52**: 1 (2020); https://doi.org/10.1007/s11082-020-02306-8
83. C. Vidyasagar, Y. Arthoba Naik, T. Venkatesha, and R. Viswanatha, *Nano-Micro Letters*, **4**: 73 (2012); https://doi.org/10.1007/BF03353695
84. K. Khojier and A. Behju, *International Journal of Nano Dimension*, **2**, Iss. 3: 185 (2012).
85. M. Heinemann, B. Eifert, and C. Heiliger, *Physical Review B*, **87**, Iss. 11: 115111 (2013); https://doi.org/10.1103/PhysRevB.87.115111
86. A. S. Zoolfakar, R. A. Rani, A. J. Morfa, A. P. O'Mullane, and K. Kalantar-Zadeh, *Journal of Materials Chemistry C*, **2**, Iss. 27: 5247 (2014); https://doi.org/10.1039/C4TC00345D
87. G. Fritz-Popovski, F. Sosada-Ludwikowska, A. Köck, J. Keckes, and G. A. Maier, *Sci. Rep.*, **9**, Iss. 1: 807 (2019); https://doi.org/10.1038/s41598-018-37172-8
88. L. Yuan, Y. Wang, R. Mema, and G. Zhou, *Acta Materialia*, **59**, Iss. 6: 2491 (2011); https://doi.org/10.1016/j.actamat.2010.12.052
89. I. A. Ezenwa, *Research Journal of Chemical Sciences*, **2**: Iss. 3: 26 (2012); https://www.isca.me/rjcs/Archives/v2/i3/5.ISCA-RJCS-2011-252%20Done.php
90. P. Ooi, S. Ng, M. Abdullah, H. A. Hassan, and Z. Hassan, *Materials Chemistry and Physics*, **140**, Iss. 1: 243 (2013); https://doi.org/10.1016/j.matchemphys.2013.03.028
91. R. D. Prabu, S. Valanarasu, V. Ganesh, M. Shkir, S. AlFaify, A. Kathalingam, S. Srikumar, and R. Chandramohan, *Materials Science in Semiconductor Processing*, **74**: 129 (2018); https://doi.org/10.1016/j.mssp.2017.10.023
92. D. Ozaslan, O. Erken, M. Gunes, and C. Gumus, *Physica B: Condensed Matter*, **580**: 411922 (2020); https://doi.org/10.1016/j.physb.2019.411922

93. Y. H. Ribeiro, J. D. S. Pereira, D. G. David, and M. V. da Silva, *Thin Solid Films*, **757**: 139381 (2022); https://doi.org/10.1016/j.tsf.2022.139381
94. K. Khojier, H. Savaloni, and Z. Sadeghi, *Journal of Theoretical and Applied Physics*, **8**: 1 (2014); https://doi.org/10.1007/s40094-014-0116-x
95. F. A. Akgul, G. Akgul, N. Yildirim, H. E. Unalan, and R. Turan, *Materials Chemistry and Physics*, **147**, Iss. 3: 987 (2014); https://doi.org/10.1016/j.matchemphys.2014.06.047
96. M. Mabrouki, *Materials Today: Proceedings*, **13**: 771 (2019); https://doi.org/10.1016/j.matpr.2019.04.039
97. A. A. Baqer, K. A. Matori, N. M. Al-Hada, H. M. Kamari, A. H. Shaari, E. Saion, and J. L. Y. Chyi, *Journal of Materials Science: Materials in Electronics*, **29**: 1025 (2018); https://doi.org/10.1007/s10854-017-8002-3
98. A. H. Mashhad-Toroghi, N. Shahtahmasebia, E. Azhira, P. Madahia, and M. Mashreghi, *Proceedings of the 4th International Conference on Nanostructures (ICNS4)* (IR Iran: Kish Island: 2012), p. 12–14.
99. G. Tunell, E. Posnjak, and C. Ksanda, *Zeitschrift für Kristallographie — Crystalline Materials*, **90**, Iss. 1–6: 120 (1935); https://doi.org/10.1524/zkri.1935.90.1.120
100. S. Esbrink and L.-J. Norrby, *Acta Crystallographica Section B: Structural Crystallography and Crystal Chemistry*, **26**, Iss. 1: 8 (1970); https://doi.org/10.1107/S0567740870001838
101. D. Volanti, D. Keyson, L. Cavalcante, A. Z. Simxes, M. Joya, E. Longo, J. A. Varela, P. Pizani, and A. Souza, *Journal of Alloys and Compounds*, **459**, Iss. 1–2: 537 (2008); https://doi.org/10.1016/j.jallcom.2007.05.023
102. G. Pezzotti, *Journal of Applied Physics*, **113**, Iss. 21: 8 (2013); https://doi.org/10.1063/1.4803740
103. B. Balamurugan, B. Mehta, D. Avasthi, F. Singh, A.K. Arora, M. Rajalakshmi, G. Raghavan, A. Tyagi, and S. Shivaprasad, *Journal of Applied Physics*, **92**, Iss. 6: 3304 (2002); https://doi.org/10.1063/1.1499752
104. N. Touka, D. Tabli, and K. Badari, *Journal of Optoelectronics and Advanced Materials*, **21**, Iss. 12: 698 (2019).
105. M. L. Zeggar, M. Aida, and N. Attaf, *Journal of New Technology and Materials*, **277**, Iss. 1747: 1 (2014).
106. S. B. Sadale, S. B. Patil, A. M. Teli, H. Masegi, and K. Noda, *Solid State Sciences*, **123**: 106780 (2022); https://doi.org/10.1016/j.solidstatesciences.2021.106780
107. D. S. Che Halin, I. A. Talib, A. R. Daud, and M. A. A. Hamid, *Materials Science Forum*, **819**: 189 (2015); https://doi.org/10.4028/www.scientific.net/MSF.819.189
108. Y. Liu, J. Zhang, W. Zhang, W. Liang, B. Yu, and J. Xue, *Journal of Wuhan University of Technology—Mater. Sci. Ed.*, **30**, Iss. 1: 92 (2015); https://doi.org/10.1007/s11595-015-1106-9
109. U. Akgul, K. Yildiz, and Y. Atici, *The European Physical Journal Plus*, **131**: 1 (2016); https://doi.org/10.1140/epjp/i2016-16089-3
110. L. Huang, S. Yang, T. Li, B. Gu, Y. Du, Y. Lu, and S. Shi, *Journal of Crystal Growth*, **260**, Iss. 1–2: 130 (2004); https://doi.org/10.1016/j.jcrysgro.2003.08.012
111. A. Ravichandran, K. Dhanabalan, R. Chandramohan, A. Vasuhi, and P. Parameswaran, *International Journal of Information Research and Review*,

1: 007 (2014).
112. F. Mugwang'a, P. Karimi, W. Njoroge, O. Omayio, and S. Waita, *International Journal of Thin Films Science and Technology*, **2**, Iss. 1: 15 (2013).
113. L. D. L. S. Valladares, D. H. Salinas, A. B. Dominguez, D. A. Najarro, S. Khondaker, T. Mitrelias, C. Barnes, J. A. Aguiar, and Y. Majima, *Thin Solid Films*, **520**, Iss. 20: 6368 (2012); https://doi.org/10.1016/j.tsf.2012.06.043
114. W. Zheng, Y. Chen, X. Peng, K. Zhong, Y. Lin, and Z. Huang, *Materials*, **11**, Iss. 7: 1253 (2018); https://doi.org/10.3390/ma11071253
115. X. Zhang, Z. Li, and J. Fan, *Materials Science in Semiconductor Processing*, **137**: 106227 (2022); https://doi.org/10.1016/j.mssp.2021.106227
116. T. Çayir Taşdemirci, *Electronic Materials Letters*, **16**: 239 (2020); https://doi.org/10.1007/s13391-020-00205-4
117. M. R. Johan, M. S. M. Suan, N. L. Hawari, and H. A. Ching, *Int. J. Electrochem. Sci.*, **6**, Iss. 12: 6094 (2011); https://doi.org/10.1016/S1452-3981(23)19665-9
118. N. Al Armouzi, M. Manoua, H. S. Hilal, A. Liba, and M. Mabrouki, *Processes*, **10**, Iss. 7: 1277 (2022); https://doi.org/10.3390/pr10071277
119. H. B. Saвd, M. Ajili, S. Dabbabi, and N. T. Kamoun, *Superlattices and Microstructures*, **142**: 106508 (2020); https://doi.org/10.1016/j.spmi.2020.106508
120. O. Abdelouahab, Rahmane Saâd, Ben Messaoud Ouarda, K. Aicha, and S. Mostefa, *Iranian Journal of Materials Science and Engineering*, **19**, Iss. 1: (2022); https://doi.10.22068/ijmse.2582
121. L. Chabane, N. Zebbar, M. L. Zeggar, M. Aida, M. Kechouane, M. Trari, *Materials Science in Semiconductor Processing*, **40**: 840 (2015); https://doi.org/10.1016/j.mssp.2015.07.080
122. S. Shariffudin, S. Khalid, N. Sahat, M. Sarah, and H. Hashim, *IOP Conference Series: Materials Science and Engineering*, **99**, Iss. 1: 012007 (2015); https://doi.10.1088/1757-899X/99/1/012007
123. V. Bhuse, P. Hankare, K. Garadkar, and A. Khomane, *Materials Chemistry and Physics*, **80**, Iss. 1: 82 (2003); https://doi.org/10.1016/S0254-0584(02)00306-1
124. S. A. M. H. M. Ali, *Journal of Multidisciplinary Engineering Science Studies*, **2**: 532 (2016).
125. K. Kamli, Z. Hadef, B. Chouial, and B. Hadjoudja, *Surface Engineering*, **35**, Iss. 1: 86 (2019); https://doi.org/10.1080/02670844.2018.1475052
126. O. Reyes-Vallejo, J. Escorcia-García, and P. Sebastian, *Materials Science in Semiconductor Processing*, **138**: 106242 (2022); https://doi.org/10.1016/j.mssp.2021.106242
127. V. Chawla, N. Sardana, H. Kaur, A. Kumar, R. Chandra, and S. Mishra, *Applied Surface Science*, **504**: 144369 (2020); https://doi.org/10.1016/j.apsusc.2019.144369
128. L. V. Devi, S. Sellaiyan, S. Sankar, and K. Sivaji, *Materials Research Express*, **5**, Iss. 2: 024002 (2018); https://doi.10.1088/2053-1591/aaa7a3
129. I. Singh, S. Dey, S. Santra, K. Landfester, R. Muñoz-Espí, and A. Chandra, *ACS Omega*, **3**, Iss. 5: 5029 (2018).
130. N. Sankar, V. Sankaranarayanan, L. Vaidhyanathan, G. Rangarajan, R. Srinivasan, K. Thomas, U. Varadaraju, and G. S. Rao, *Solid State Communications*, **67**, Iss. 4: 391 (1988); https://doi.org/10.1016/0038-1098(88)91051-4
131. Bahaa M. Abu-Zied, Salem M. Bawaked, Samia A. Kosa, and Wilhelm Schwieger, *Int. J. Electrochem. Sci.*, **11**, Iss. 3: 2230 (2016);

https://doi.org/10.1016/S1452-3981(23)16097-4
132. Bahaa M. Abu-Zied, Salem M. Bawaked, Samia A. Kosa, and Wilhelm Schwieger, *Int. J. Electrochem. Sci*, **11**, Iss. 2: 1568 (2016); https://doi.org/10.1016/S1452-3981(23)15942-6
133. D. Wang, Y. Wang, T. Jiang, H. Jia, and M. Yu, *Journal of Materials Science: Materials in Electronics*, **27**: 2138 (2016); https://doi.org/10.1007/s10854-015-4003-2
134. C. Meneses, J. Duque, L. Vivas, and M. Knobel, *Journal of Non-Crystalline Solids*, **354**, Iss. 42–44: 4830 (2008); https://doi.org/10.1016/j.jnoncrysol.2008.04.025
135. S. Baig, P. Kumar, J. Ngai, Y. Li, and S. Ahmed, *Chem. Phys. Chem.*, **21**, Iss. 9: 895 (2020); https://doi.org/10.1002/cphc.202000005
136. M. Ariëns, L. van de Water, A. I. Dugulan, E. Brück, and E. J. Hensen, *Journal of Catalysis*, **405**: 391 (2022); https://doi.org/10.1016/j.jcat.2021.12.013
137. W. Wang, Z. Li, W. Zheng, J. Yang, H. Zhang, and C. Wang, *Electrochemistry Communications*, **11**, Iss. 9: 1811 (2009); https://doi.org/10.1016/j.elecom.2009.07.025
138. H. Absike, M. Hajji, H. Labrim, A. Abbassi, and H. Ez-Zahraouy, *Superlattices and Microstructures*, **127**: 128 (2019); https://doi.org/10.1016/j.spmi.2017.12.038
139. S. Masudy-Panah, K. Radhakrishnan, H. R. Tan, R. Yi, T. I. Wong, and G. K. Dalapati, *Solar Energy Materials and Solar Cells*, **140**: 266 (2015); https://doi.org/10.1016/j.solmat.2015.04.024
140. R. M. Thyab, M. A. Al-Hilo, F. A. Yasseen, H. Alshater, E. G. Blall, and M. A. Abdel-Lateef, *NeuroQuantology*, **20**, Iss. 3: 99 (2022); https://doi.10.14704/nq.2022.20.3.NQ22048
141. J. H. Bae, J. H. Lee, S. P. Park, T. S. Jung, H. J. Kim, D. Kim, S.-W. Lee, K.-S. Park, S. Yoon, and I. Kang, *ACS Applied Materials & Interfaces*, **12**, Iss. 34: 38350 (2020).
142. A. Yildiz, Ş. Horzum, N. Serin, and T. Serin, *Applied Surface Science*, **318**: 105 (2014); https://doi.org/10.1016/j.apsusc.2014.01.118
143. D. Tabli, D. N. Touka, K. Baddari, and N. Selmi, *Advances in Materials Science*, **22**, Iss. 3: 5 (2022); https://doi.org/10.2478/adms-2022-0009
144. D. Tabli, N. Touka, K. Baddari, and N. Selmi, *Advances in Materials Science*, **22**, Iss. 3: 5 (2022); https://doi.org/10.2478/adms-2022-0009
145. H. Siddiqui, M. Qureshi, and F. Z. Haque, *Materials Letters*, **275**: 128090 (2020); https://doi.org/10.1016/j.matlet.2020.128090
146. H. Siddiqui, M. R. Parra, M. Qureshi, M. Malik, and F. Z. Haque, *Journal of Materials Science*, **53**, Iss. 12: 8826 (2018); https://doi.org/10.1007/s10853-018-2179-6
147. T. V. Thi, A. K. Rai, J. Gim, and J. Kim, *Applied Surface Science*, **305**: 617 (2014); https://doi.org/10.1016/j.apsusc.2014.03.144
148. C.-Y. Chiang, Y. Shin, and S. Ehrman, *Journal of The Electrochemical Society*, **159**, Iss. 2: B227 (2011); https://doi.10.1149/2.081202jes
149. F. Z. Chafi, L. Bahmad, N. Hassanain, B. Fares, L. Laanab, and A. Mzerd, *arXiv preprint arXiv*: 1807.09697 (2018); https://doi.org/10.48550/arXiv.1807.09697
150. L. V. Devi, T. Selvalakshmi, S. Sellaiyan, A. Uedono, K. Sivaji, and S. Sankar, *Journal of Alloys and Compounds*, **709**: 496 (2017);

https://doi.org/10.1016/j.jallcom.2017.03.148
151. S. Bhuvaneshwari and N. Gopalakrishnan, *Journal of Alloys and Compounds*, **654**: 202 (2016); https://doi.org/10.1016/j.jallcom.2015.09.046
152. Sayantan Das and T. L. Alford, *Journal of Applied Physics*, **113**: 244905 (2013); https://doi.org/10.1063/1.4812584
153. A. Menazea and A. M. Mostafa, *Journal of Environmental Chemical Engineering*, **8**, Iss. 5: 104104 (2020); https://doi.org/10.1016/j.jece.2020.104104
154. S. Vidhya, O. Balasundaram, and M. Chandramohan, *Journal of Optoelectronics and Advanced Materials*, **17**: 963 (2015).
155. J. Wu, K. Hui, K. Hui, L. Li, H.-H. Chun, and Y. Cho, *Journal of Materials Science: Materials in Electronics*, **27**: 1719 (2016); https://doi.org/10.1007/s10854-015-3945-8
156. F. Bayansal, Y. Gülen, B. Şahin, S. Kahraman, and H. Çetinkara, *Journal of Alloys and Compounds*, **619**: 378 (2015); https://doi.org/10.1016/j.jallcom.2014.09.085